A Novel Carbon Nanotube-Biomedical Polymer Composite Platform for Bioelectrochemical Applications

S. Ounnunkad[*], A.I. Minett[*], B.D. Fleming[**], A.M. Bond[**] and G.G. Wallace[*]

[*]ARC Centre of Excellence for Electromaterials Science,
Intelligent Polymer Research Institute, University of Wollongong, Innovation Campus,
AIIM Building, Squires Way, Fairy Meadow, NSW 2519, Australia,
suriyacmu@yahoo.com, aminett@uow.edu.au, gwallace@uow.edu.au
[**] School of Chemistry, Monash University, Clayton, Victoria 3800, Australia,
barry.fleming@sci.monash.edu.au, Alan.Bond@sci.monash.edu.au

ABSTRACT

The construction of and the electrochemical characteristics of a novel freestanding biomedical polymer-single walled carbon nanotube (SWCNT) nanocomposite electrode, formed via an intercalation process, have been described. The SWCNT Buckypapers are prepared from SWCNT dispersion solution via a filtration process, followed by soaking in a 5%w/v insulating poly(styrene-β-isobutylene-β-styrene) (SIBS) solution. The intercalated platforms represent randomly dispersed CNT bundles and individual CNTs which are partially surrounded by an insulating polymer. This arrangement leads to an improvement in the Faradaic to capacitive charging ratio, relative to electrodes derived from non-intercalated samples. The electrochemical behaviour of freestanding SIBS intercalated SWCNT Buckyelectrodes have been investigated via analysis of DC and Fourier transformed AC voltammetries in order to determine the composites ability to serve as an electrode platform. In comparison with the bare sample, significantly faster electron transfer reaction rates and improved Faradaic to capacitive background charging current ratios, suggest that the devices made from this novel nanocomposite electrode should offer improved performance in electroanalytical applications, and possibility also in bio-/chemo-sensors, biofuel cell type devices and as a biocompatible platform for cell culturing.

Keywords: poly(styrene-β-isobutylene-β-styrene), single-walled carbon nanotube, Buckypaper, electron transfer, DC voltammetry, FT-AC voltammetry

1 INTRODUCTION

Since their popularisation in 1991, carbon nanotubes (CNTs) have attracted a tremendous amount of attention due to their extraordinary physical, chemical, and mechanical properties [1]. They also have high electrochemically accessible surface areas and good electrical conductance, two important parameters applicable to electroanalytical devices [2-3]. CNTs can be manipulated into many different kinds of architectures or platforms such as CNT modified electrodes [4], layer-by-layer films [5], aligned CNTs [4], fibres [6] and free standing films (Buckypaper) [7].

Self-supporting carbon nanotube mats, are utilized today in an increasing number of applications including artificial muscles [8], bio-electrode platforms, for cell cultures [9], sensors [10], hydrogen storage materials [11], supercapacitors [12-13], and anode materials in lithium ion batteries [14]. Simple nanocomposites of this architecture can be made via adding biopolymers [9] or conducting polymers [13] to improve biocompatibility or electrochemical performances and via intercalating organic polymers [7, 15] to enhance the mechanical strength.

In this work, the fabrication and electrochemical properties of the novel biomedical polymer-SWCNT nanocomposite electrode platform formed via a polymer intercalation process has been first investigated and described. The electrochemical improvement of such composite electrodes is surprisingly found after intercalation with an insulating polymer. In comparison with bare Buckypaper (BP), the polymer intercalated BP has a significantly improved Faradaic response and an enhanced Faradaic to background charging current ratio. This modification process also results in a faster electron transfer rate for oxidation of the reactant at the novel electrode interface.

2 EXPERIMENTAL DETAILS

2.1 Sample Preparation

Carbon nanotube freestanding films were prepared by dispersion of SWCNT (CNI, batch no. P0343) in an aqueous solution of Triton X-100. A SWCNT dispersion solution was prepared by mixing 120 mg of SWCNT in 1 % v/v aqueous solutions of Triton-X100 (240 ml), using horn sonication (2h) and then bath sonication (2h). The dispersability of SWCNT soot using this method was monitored using an optical microscope. The dispersion was then filtered using a hydrophobic PVDF membrane (pore size = 0.22μm). The resulting CNT freestanding film was first washed with Milli-Q water, followed by ethanol until the foam disappeared, indicating that the un-adsorbed

surfactant was removed. The BP was allowed to dry overnight at 60°C.

2.2 Intercalation Process

A 5%w/v biomedical polymer, poly(styrene-β-isobutylene-β-styrene) (SIBS) solution was prepared using toluene as a solvent. A raw BP was cut into many small strips (0.5 x 2.5 cm^2 in size) and were soaked into the SIBS for the desired time, 72hrs. After soaking, the SIBS-intercalated BP strips (SIBS-BP) were rinsed with the solvent and left to dry overnight at 60°C. The polymer uptake was determined as a weight % per BP sample both before and after the intercalation process using a microbalance.

2.3 Morphological and Voltammetric Studies

The morphology of the BP architecture was investigated using a JOEL Scanning Electron Microscope. A conventional three-electrode cell was employed for all electrochemical measurements, with an Ag/AgCl (saturated NaCl) electrode used as the reference electrode and a platinum wire auxiliary electrode. SIBS-BP was used as the working electrode. Electrochemical properties of a prepared BP electrode (BPE) were measured by using both Direct Current voltammetry (DC) and Fourier Transformed large-amplitude Alternating Current voltammetry (FT-AC).

3 RESULTS AND DISCUSSION

Scanning electron microscopy (SEM) images of a bare BP and SIBS-BP are shown in Figure 1. Figure 1 reveals the morphology of BP surface, which consists of randomly ordered individual CNTs/CNT bundles [7]. The sheet has a density of about 0.93 g/cm^3 at an intercalating SIBS polymer composition uptake of about 30% (Figure 1b) while a raw BP sample has a density of 0.71 g/cm^3 (Figure 1a). Illustrated in Figure 1(b) shows the microstructure and packing nature of individual CNTs and/or CNT bundles containing an intercalating polymer. This emphasizes that the SIBS polymer occupies an interbundle/interstitial free volume of the SWCNT network BP. Polymer occupation into a BP after intercalation is confirmed using a mass difference between raw and intercalated BP and an increase in density (31%). Figure 1b also shows that after intercalation, the porous nature of the surface of the raw BP is maintained.

Figures 1(c) and 1(d) represent a simplification of the two electrode architectures in an effort to simply the electrochemical explanation of results. As established in Figure 1c, the raw BP forms a structure possessing individual CNTs/CNTs bundles in which there is a very high porosity available to form a large double layer capacitive film. It is proposed that there is a completely overlapping diffusion layer for each CNT nanodomain (ie. no CNT nano-/micro-domain separation) which transforms into a planar diffusion layer. It behaves as a flat electrode possessing only one diffusion layer over the entire electrode surface and has a very high charging current. Figure 1d shows after intercalation the polymer-SWCNT BP acts as a random array of individual CNTs/CNT bundles surrounded by intercalating non-conducting polymer and the interstitial pores between individual CNTs/CNT bundles are also occupied. The architecture represents a random edge plane and basal plane-like defect nanoarray on the electrode surface. There are significant spaces between each nanodomain revealing partially overlapping small diffusion layers of each CNT nano-/micro-domains on the surface.

Figure 2 shows cyclic voltammograms of (a) a raw BPE and (b) a SIBS-BPE obtained in 1mM ferrocenecarboxylic acid (FMCA) in pH7.4 phosphate buffer electrolyte media containing 0.1M KCl. Figure 2a shows a voltammetric response with a large capacitive background and little or no Faradaic response. Peak-to-peak separation (ΔE_P) of a raw BP is about 290 mV and the voltammetry shows a higher charging current density. Some of bare BP do not show any oxidation of FMCA, indicating an inactive electrode surface towards the reactants. In Figure 2b, there is negligible shift in either the oxidation or reduction peak potentials when the scan rate is varied from 5 to 200 mVs^{-1}. The ΔE_P value of 70 ± 15 mV for all scan rates suggests Nernstian behaviour with the electron transfer rate at the SIBS intercalated BP being much faster than at a bare electrode [16]. The linear plot of peak height versus the square root of scan rate (inset) indicates that the $FMCA^{0/+}$ process is diffusion-controlled at a SIBS-BPE.

In addition after SIBS intercalation, the SIBS intercalated BP has a significant decrease in the background charging current and a significant improvement in redox response and kinetics at such an electrode as seen with a decrease in the ΔE_P value. This suggestion of a faster electron transfer rate of a redox probe at a SIBS-BPE

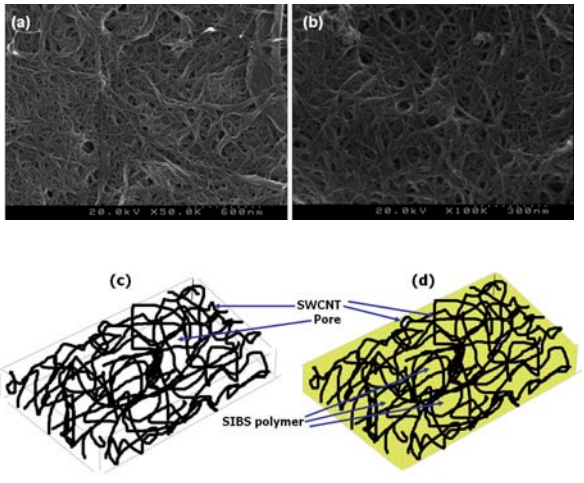

Figure 1: SEM images for (a) raw BP and (b) SIBS-BP and schematic of proposed structure for (c) raw BP and (d) SIBS-BP respectively.

NSTI-Nanotech 2009, www.nsti.org, ISBN 978-1-4398-1783-4 Vol. 2, 2009

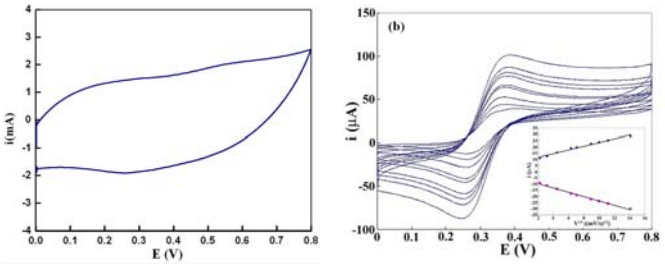

Figure 2: DC cyclic voltammograms for oxidation of 1mM FMCA at (a) raw BPE and (b) SIBS-BPE; inset of peak currents versus square root of scan rate (5-200mVs^{-1}).

indicates that SIBS may block the interaction of the reactant (FMCA) to the basal-plane like defects of CNTs (slower kinetic rate) whilst allowing more interaction at the edge-plane sites of the electrode surface (higher kinetic rate) [17-19].

Figure 2 additionally shows that the raw BP electrode reveals no redox response while the intercalated sample data clearly shows a strongly reversible redox couple set of oxidation and reduction peaks with a small peak separation, indicating fast electron transfer kinetics. The raw material BPE has a large surface area with very high porosity, capable of forming a very high magnitude capacitive double layer. This results in a dominant non-Faradaic current or very low Faradaic to background charging current ratio, as observed in Figure 2a. A second influence is that the BPE contains both basal-plane and edge-plane like defects possessing different reactivities. There is competition between interactions at basal plane-like defects (slow kinetics) and at edge plane-like defects (fast kinetics) which are highlighted in the voltammograms characteristics [17-19]. In the BPE sample, it can be expected that there is an abundance of basal-plane like defects dominating over the edge-plane like defects. The large double layer capacitance seen in the response of this BP electrode is generated at these basal-plane sites. It follows that the redox probe interacts at the basal-plane site defects rather than at the edge-plane reactive sites.

In the SIBS-BPE case, the non-conducting organic polymer intercalates into the free volume space and non-covalently functionalises the non-polar part of the nanotubes (basal plane like defects) whilst leaving available more edge-plane sites on the electrode surface. Therefore, the redox probe in the electrolyte solution interacts at the highest reactivity part at the electrode surface whilst the interaction at slow kinetic pathways (basal plane) is limited. This provides a significantly improved Faradaic to background charging current ratio.

Moreover, we make the assumption that the BPE represents a random microelectrode array to explain the electrochemical behaviour of the SIBS-BPE. At the BPE surface the random CNT bundles can be represented as an array of nano-/micro-electrodes (individual CNTs/CNT bundles) surrounded by the SIBS polymer. A planar diffusion layer occurs over the individual nano-/micro-electrodes on the electrode surface (raw BP) with an overlapping diffusion layer from each microelectrode. These overlapping diffusion layers result in an equivalent cyclic voltammogram to that of a planar flat electrode. Intercalation of the SIBS polymer limits the amount of overlapping reactant sites, creating an array of discrete nano-/micro-electrodes. The cyclic voltammograms observed in Figure 2b, is therefore a combination from each contribution of each nano-/micro-electrode. This construct provides a significantly reduced capacitive background current compared to the raw BPE, suggesting that such devices may offer improved signal to noise resolution in electro-analytical measurements [20-22].

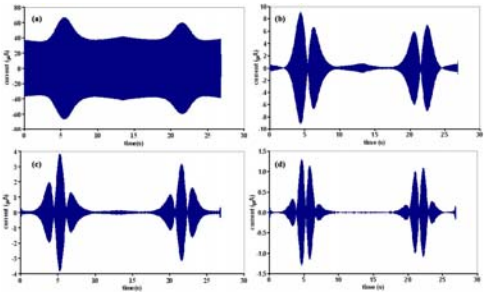

Figure 3: FT-AC voltammograms obtained for fundamental (a), second (b), third (c), and fourth (d) harmonics for oxidation of 1mM FMCA at a SIBS-BP. Condition employed: a sine wave, f = 35 Hz, ΔE = 80 mV, v =59.60 mVs^{-1}, E_{start} = 0 mV, and E_{switch} = 800 mV.

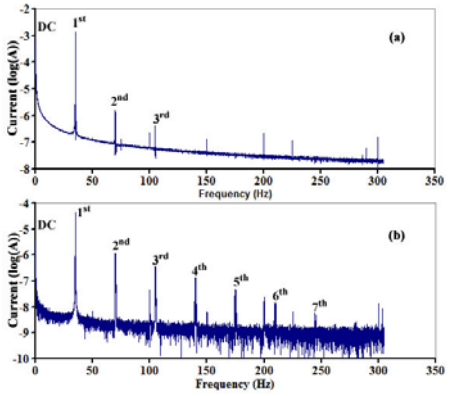

Figure 4: Log power spectra of FT-AC voltammograms obtained for oxidation of 1mM FMCA for (a) raw BP and (b) SIBS-BP, respectively. Conditions same as Figure 3.

Large-amplitude Fourier Transformed alternating current voltammetry (FT-AC) is a powerful AC voltammetric methodology which provides a high sensitivity to fast electron transfer processes, promoting higher AC Faradaic harmonic responses [23]. This technique offers significantly more information than DC voltammetry alone and provides an insight into the resistance, capacitance, and kinetics at the electrode surface, all obtained from a single experiment. A set of large-amplitude AC voltammetric components after Fourier

transformation is shown in Figure 3(a-d). The fundamental (a), second (b), third (c), and fourth (d) harmonics are respectively shown. In this experiment, the sine wave function (f = 35 Hz, ΔE =80 mV, v =59.60 mVs^{-1}) is superimposed onto a DC waveform to obtain the FT-AC cyclic voltammogram [24]. In FT-ACV the currents of each component are plotted using a time domain rather than the normal DC potential (DC voltammetry). The first Faradaic region detected for each harmonic represents the oxidation of FMCA to $FMCA^+$ and the second region is of the reduction of $FMCA^+$ to FMCA. Each ac component reveals electrode properties close to an ideal one-electron reversible process [25]. The reversible potentials (E_m) from each harmonic are close to the E_m value derived from DC cyclic voltammetry (314 mV). Thus, the reversibility of the $FMCA^{0/+}$ redox process can be easily observed under AC voltametric conditions.

Figures 4 shows the log power spectra after Fourier transform for the voltammograms of a redox probe, FMCA at both the bare BPE (4a) and SIBS-BPE (4b) respectively. It is clearly seen that after the intercalation process the kinetics at the SIBS-BPE is vastly improved, presenting higher-order AC harmonic responses up to the seventh harmonic compared to the BPE showing a slower electron transfer showing first to third harmonics. This confirms that intercalating SIBS does improve the kinetics at such an electrode architecture, providing faster electron transfer compared to normal BP. From this evidence, the SIBS-BP can be used as an electrochemical sensing platform in electroanalysis, providing higher signal to noise performance.

4 CONCLUSIONS

Intercalating the SIBS biopolymer promotes an improvement of the kinetics, faster electron transfer of FMCA at a novel SIBS-BP electrode compared to the raw BPE. The structure of SIBS intercalated BP forms a random array of nano-/micro-electrode domains derived from individual CNTs/CNT bundles on the exposed surfaces. FT-AC voltammetry confirmed the fast electron transfer reaction of the redox species $FMCA^{0/+}$ at the novel BPE surface. In the future it is hoped that this novel architecture can be effectively used in chemical or biochemical sensing applications.

5 ACKNOWLEDGEMENTS

The ongoing financial support of the Australian Research Council is gratefully acknowledged. S.O. acknowledges award of a PhD Scholarship in Nanoscience and Nanotechnology (Nanodevices) by Higher Educational Strategic Scholarships for Frontier Research Network from the Commission on Higher Education, Ministry of Education, Royal Thai Government. A.I.M. acknowledges a QEII Research Fellowship from the ARC.

REFERENCES

[1] S. Iijima, *Nature*, 354, 56, 1991.
[2] P.M. Ajayan, *Chem. Rev.*, 99, 1787, 1999.
[3] L. Dai (Ed.), "Carbon Nanotechnology", Elsevier, 2006.
[4] J. Wang *et. al.*, *Anal. Chem.*, 74, 1993, 2002.
[5] G.A. Rivas *et. al.*, *Talanta*, 71, 270, 2007.
[6] C. Lynam *et. al.*, *Adv. Mater.*, 19(9), 1244-1248, 2007
[7] C.J. Frizzell *et. al.*, *Phys. Rev. B*, 72, 245420, 2005.
[8] U. Vohrer *et. al.*, *Carbon*, 42, 1159-1164, 2004.
[9] P.G. Whitten *et. al.*, *J. Biomed. Mater. Res. Part B: Appl. Biomater.*, 82B, 37-43, 2007.
[10] P. Dharap *et. al.*, *Nanotechnology*, 15, 379-382, 2004.
[11] C. Liu *et. al.*, *Science*, 286, 1127-1129, 1999.
[12] T. Liu *et. al.*, *Carbon* 41, 2427-2451, 2003.
[13] J. Oh *et. al.*, *Synth. Met.*, 158, 638-341, 2008.
[14] A.S. Claye *et. al.*, *J. Electrochem. Soc.*, 147, 2845-2852, 2000.
[15] J.N. Coleman *et. al.*, *Appl. Phys. Lett.*, 82, 1682-1684, 2003.
[16] K. Gong *et. al.*, *Angew. Chem. Int. Ed.*, 47, 5446-5450, 2008.
[17] M.C. Henstridge *et. al.*, *Electroanalysis*, 20(5), 498-506, 2008.
[18] A.F. Holloway *et. al.*, *J. Solid State Electrochem.*, 12, 1337-1348, 2008.
[19] N. Punbusayakul *et. al.*, *Electrochem. Solid State Lett.*, 10(5) F13-F17, 2007.
[20] J. Guo *et. al.*, *Anal. Chem.*, 81(1), 130-13, 2009.
[21] L. Xiao *et. al.*, *Sens. Actuator B-Chem.*, 133, 118-127, 2008.
[22] C.N. LaFratta *et. al.*, *Chem. Rev.*, 108, 614-637, 2008.
[23] C.-Y. Lee, A.M. Bond, *Anal. Chem.*, *81,* 584-594, 2009.
[24] A.M. Bond *et. al.*, *Anal. Chem.*,77, 186A, 2005.
[25] B.D. Fleming *et. al.*, *Anal. Chem.*, 77, 3502-3510, 2005.